

# A Luttinger Liquid Core Inside Helium-4 Filled Nanopores

Adrian Del Maestro

*Department of Physics, University of Vermont, Burlington, VT 05405, USA*

(Dated: October 31, 2018)

## Abstract

As helium-4 is cooled below 2.17 K it undergoes a phase transition to a fundamentally new state of matter known as a superfluid which supports flow without viscosity. This type of dissipationless transport can be observed by forcing helium to travel through a narrow constriction that the normal liquid could not penetrate. Recent experiments have highlighted the feasibility of fabricating smooth pores with nanometer radii, that approach the truly one dimensional limit where it is believed that a system of bosons (like helium-4) may have startlingly different behavior than in three dimensions. The one dimensional system is predicted to have a linear hydrodynamic description known as Luttinger liquid theory, where no type of long range order can be sustained. In the limit where the pore radius is small, Luttinger liquid theory would predict that helium inside the channel behaves as a sort of quasi-supersolid with all correlations decaying as power-law functions of distance at zero temperature. We have performed large scale quantum Monte Carlo simulations of helium-4 inside nanopores of varying radii at low temperature with realistic helium-helium and helium-pore interactions. The results indicate that helium inside the nanopore forms concentric cylindrical shells surrounding a core that can be fully described via Luttinger liquid theory and provides insights into the exciting possibility of the experimental detection of this intriguing low dimensional state of matter.

## I. INTRODUCTION

As the spatial dimension of an interacting many-body system is reduced, both thermal and quantum fluctuations are enhanced, providing a fascinating arena for the study of complex phenomena. It is well known that in strictly one dimension, there is no broken continuous symmetry but instead the persistence of only quasi-long range order characterized by power-law decay of correlation functions. The simplest example of a model displaying these features is the one dimensional (1d) non-relativistic Galilean invariant Bose gas with delta function interactions. The ground state of this model has been known for almost fifty years and can be solved exactly using the Bethe Ansatz<sup>1</sup>. An alternative approach, based on the concept of a low dimensional harmonic fluid<sup>2-5</sup> was first understood to be universal by Haldane<sup>6,7</sup> with the techniques formalized in these seminal works now generally known as bosonization and Luttinger liquid (LL) theory. The combination of these two approaches indicate that there is no well defined quantum phase transition at zero temperature as a function of the strength of the interactions in 1d. As interactions are increased, the system crosses over from a regime dominated by phase fluctuations, to one with tendencies towards density wave order. Likewise, there is no phase transition as a function of temperature.

Historically, the experimental study of low dimensional physics has been confined to fermionic systems such as insulating spin chains and quantum wires<sup>8</sup> and a bosonic realization has been lacking. The identification of accessible bosonic systems is particularly relevant in light of the universal predictions of LL theory. Recently, weakly interacting ultra-cold bosonic gases consisting of laser trapped Alkali atoms confined to cigar shaped quasi-one-dimensional condensates<sup>9</sup> or rings<sup>10</sup> have been studied but it is difficult to obtain results at higher densities where the constituent atoms are more strongly interacting. The various theoretical approaches and considerations required to study such systems have been covered in detail in a recent review article<sup>11</sup>.

A considerably different approach involves the preparation of a quantum fluid of interacting bosons, such as neutral  $^4\text{He}$  in a *physically* confining geometry at high density. In fact, the ability of helium-4 cooled below  $T_\lambda = 2.17$  K (the bulk superfluid transition temperature in  $^4\text{He}$ ) to flow through a narrow constriction (superleak) is one of the original defining characteristics of the superfluid state of matter. Original experiments in this vein achieved physical confinement of helium through the quasi-1D cavernous networks of porous glasses

such as Vycor<sup>12</sup> and more recently using folded sheets of mesoporous materials<sup>13</sup>. Advances in nanofabrication techniques have culminated in a more systematic approach that has been exploited by Savard *et al.*<sup>14,15</sup> in studying  $^4\text{He}$  inside nanopores of variable radii by sculpting a pore through a  $\text{Si}_3\text{N}_4$  membrane using a transmission electron beam. Although these experiments have thus far focused on flow properties of helium in the gas phase in nanopores<sup>14</sup> and the superfluid phase for wide nanoholes<sup>15</sup> they provide a tantalizing road map for the experimental detection of a bosonic Luttinger liquid. It is thus natural to ponder a simpler equilibrium system, that can be studied numerically as a function of pore radius and temperature below  $T_\lambda$ . We expect that when the pore radius is sufficiently small, the length sufficiently long and the temperature low enough with respect to  $T_\lambda$  the  $^4\text{He}$  filled nanopore should begin to exhibit strictly 1d behavior where LL theory can be used to characterize the nature of the quasi-long-range order.

The remainder of this paper is concerned with the precise definition of *sufficiently* in the previous sentence and is organized as follows. We first identify the particulars of a theoretical model of confined helium-4 and introduce the stochastically exact numerical method employed to study its behavior. The numerical results are used to determine a phase diagram for helium inside the pore with special attention paid to the types of structures that are allowed by the Galilean invariant cylindrically symmetric confining potential. Density-density correlations inside the inner region of the pore are then analyzed in terms of Luttinger liquid theory which is introduced in an economical fashion with references provided to more complete and elaborate treatments elsewhere. The results highlight the applicability of the linear hydrodynamics of LL theory in describing helium inside nanopores and a discussion of the consequences and limitations of this finding is presented.

## II. PATH INTEGRAL SIMULATIONS OF CONFINED HELIUM-4

The finite extent and translational invariance of the van der Waals interaction between  $^4\text{He}$  atoms combined with their fundamental indistinguishability conspire to make the numerical study of quantum fluids a challenging task. Unbiased stochastically exact simulations of the quantum bosonic many-body problem in the continuum at low temperature have only recently become more feasible through the introduction of the continuous space Worm Algorithm (WA)<sup>16,17</sup>. This method builds upon the conventional Path Integral Monte Carlo

approach of Ceperley<sup>18</sup> that exploits the Feynman path integral interpretation of quantum mechanics to perform Metropolis sampling of the *worldlines* of particles in  $d+1$  dimensions. The WA extends the configuration space to include open worldlines known as *worms* that are not periodic in imaginary time and directly contribute to the single particle Matsubara Green function allowing for simulations to be performed in the grand canonical ensemble. The simulation cell is kept in thermal equilibrium with a surrounding bath with which it can exchange particles and the chemical potential  $\mu$  is an input parameter providing access to important physical observables such as the compressibility. In addition, the WA employs an efficient method via the swap operator<sup>16</sup> to directly sample the quantum statistics of identical bosons through only local exchanges of worldlines. Such exchanges are the crucial step en route to the superfluid state of matter, with the superfluid density being measured through a topological winding number; the standard technique in continuum simulations<sup>19</sup>.

We wish to perform WA simulations on a realistic physical model of the experimental single nanopore geometry discussed in the introduction with details in References 14 and 15 and thus must consider interactions between helium atoms, as well as the interactions between helium and the atoms composing the material surrounding the nanopore. Our starting point is the general microscopic many-body Hamiltonian

$$\hat{H} = \sum_{i=1}^N \left[ -\frac{1}{2m} \hat{\nabla}_i^2 + \hat{V}(\mathbf{r}_i) \right] + \sum_{i < j} \hat{v}(\mathbf{r}_i - \mathbf{r}_j) \quad (1)$$

where  $\mathbf{r}_i$  are the spatial positions of the  $N$  helium atoms and we have set  $\hbar = k_B = 1$ . The natural units of length in the nanopore systems are angstroms and in these reduced units, the mass of the helium atoms is  $m = 0.0826 \text{ \AA}^{-2} \text{K}^{-1}$ . The interaction energy between two helium atoms  $v$ , is given by the 1979 Aziz potential<sup>20</sup>

$$v(r) = \epsilon u \left( \frac{r}{r_{\min}} \right), \quad (2)$$

$$u(x) = A e^{-\alpha x} - \left( \frac{C_6}{x^6} + \frac{C_8}{x^8} + \frac{C_{10}}{x^{10}} \right) \begin{cases} e^{-(D/x-1)^2} & ; x < D \\ 1 & ; x \geq D \end{cases} \quad (3)$$

with a set of parameters inferred from both first principles calculations and experimental measurements to be  $r_{\min} = 2.9673 \text{ \AA}$ ,  $A = 5.449 \times 10^5$ ,  $\epsilon/k_B = 10.8 \text{ K}$ ,  $\alpha = 13.353$ ,  $D = 1.2413$ ,  $C_6 = 1.3732$ ,  $C_8 = 0.42538$  and  $C_{10} = 0.1781$ . This potential, shown as an inset in Figure 1, contains both hardcore repulsion for distances less than  $r_{\text{hc}} \simeq 2.64 \text{ \AA}$ , a

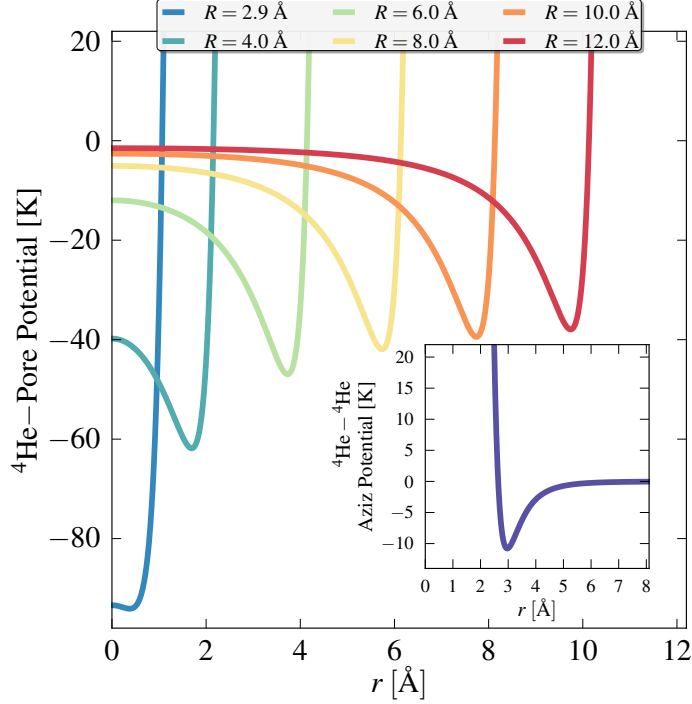


FIG. 1. The interaction potential  $V$  between helium and the walls of the nanopore constructed of amorphous  $\text{Si}_3\text{N}_4$  for various radii ranging from  $R = 2.9 \text{ \AA}$  (left) to  $R = 12.0 \text{ \AA}$  (right) calculated via Eq. (4) where  $r$  is the radial distance of a helium atom from the axis of the cylinder. The inset shows the Aziz interaction potential  $v$ , described in Eq. (2) for two helium atoms separated by a distance  $r$ .

minimum at  $r_{\min}$  and weak attraction at large separations. The external potential,  $V$  can be computed by modeling the nanopore as long cylindrical cavity carved inside a continuous medium. The potential energy of interaction of a single helium atom with the atoms of the medium can be obtained by integrating a Lennard-Jones pair potential as described in Reference 21 yielding

$$V(r; R) = \frac{\pi \varepsilon \sigma^3 n}{3} \left[ \frac{7}{32} \left( \frac{\sigma}{R} \right)^9 u_9 \left( \frac{r}{R} \right) - \left( \frac{\sigma}{R} \right)^3 u_3 \left( \frac{r}{R} \right) \right] \quad (4)$$

for a perfect cylindrical cavity of radius  $R$  where  $n$  is the number density and  $\sigma$  and  $\varepsilon$  are the Lennard-Jones parameters of the surrounding medium. The functional coefficients are

given by

$$u_9(x) = \frac{1}{240(1-x^2)^9} [(1091 + 11516x^2 + 16434x^4 + 4052x^6 + 35x^8)E(x^2) - 8(1-x^2)(1+7x^2)(97+134x^2+25x^4)K(x^2)] \quad (5)$$

$$u_3(x) = \frac{2}{(1-x^2)^3} [(7+x^2)E(x^2) - 4(1-x^2)K(x^2)] \quad (6)$$

where  $K(x)$  and  $E(x)$  are the complete elliptical integrals of the first and second kind respectively and  $r$  is the radial distance from the axis of the pore. Using the Lorentz-Berthelot mixing rules for the microscopic Lennard-Jones parameters of amorphous  $\text{Si}_3\text{N}_4$ <sup>22-24</sup> we set  $\varepsilon = 10.22$  K and  $\sigma = 2.628$  Å with  $n = 0.078$  Å<sup>-3</sup>. A plot of the pore potential for different radii is shown in Figure 1. The use of parameters for different media such as silica glass<sup>25</sup> will alter the overall energy scale and may change the excluded volume experienced by atoms inside the pore but will not qualitatively affect the findings of this study.

### III. HELIUM-4 INSIDE NANOPORES

Using this model for the interaction and confinement potentials, we have computed the low temperature thermodynamics of fluid  $^4\text{He}$  inside nanopores with lengths between  $L = 50$  and  $200$  Å and temperatures ranging from  $T = 0.5 - 2.0$  K using the WA. We imagine the nanopore to be immersed in an essentially infinite bath of helium maintained at saturated vapor pressure (SVP) which sets the chemical potential in our grand canonical simulations to be  $\mu = -7.2$  K. A wide range of cylindrical pores with radii  $R$  between  $2.9$  and  $12.0$  Å have been considered where we assume periodic boundary conditions along the axis of the cylinder.

We restrict the temperature in our simulations to be less than  $T_\lambda \simeq 2.17$  K and wish to confirm that we are studying a *low energy* quantum regime. This is most straightforwardly determined by measuring the average kinetic energy per particle in our quantum Monte Carlo (QMC) simulations as shown in Figure 2 and comparing with the temperature. We observe a general trend of decreasing kinetic energy, from more than  $30$  K per particle for  $R = 2.9$  Å to  $20$  K per particle for  $R = 12$  Å. The non-monotonic behavior observed between  $R = 2.9$  Å and  $R = 4.0$  Å can be attributed to the complete transverse confinement of helium in the narrowest pore. The minimum value of the kinetic energy observed is an order of magnitude larger than all temperatures considered and we thus conclude our simulations are

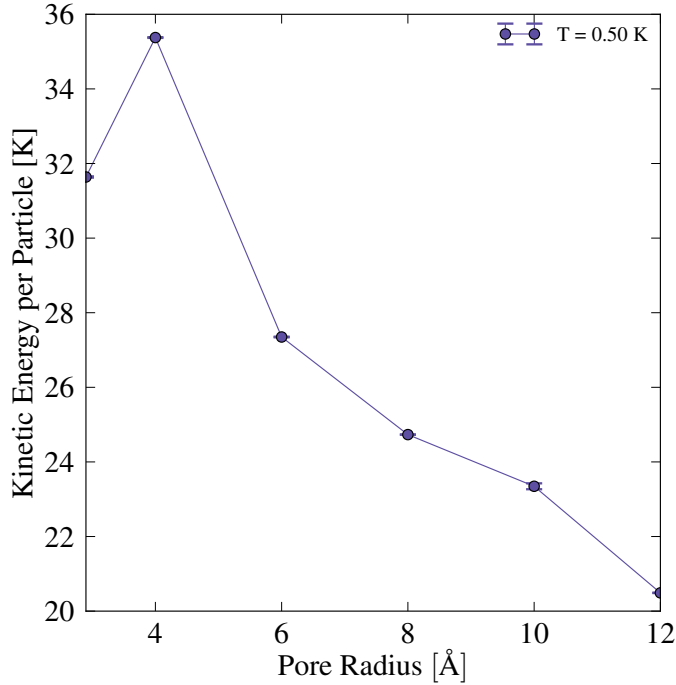


FIG. 2. The average kinetic energy per particle vs. pore radius measured via a thermodynamic estimator at low temperature ( $T = 0.5$  K) for a pore of length  $L = 100$  Å held at  $\mu = -7.2$  K.

dominated by quantum effects. Unless otherwise specified, we fix the length of the nanopore to be  $L = 100$  Å allowing three dimensional number densities to be easily converted into particle numbers (usually near 1000 helium atoms). The errorbars in Figure 2 are the result of a bootstrapping analysis of over  $10^6$  individual measurements of the kinetic energy using a thermodynamic estimator<sup>26</sup>. We have fixed the number of time slices (the discretization of the imaginary time interval corresponding to the inverse temperature) to be 125 per degree kelvin. Possible Trotter error introduced by using a finite imaginary time step  $\Delta\tau$  has been analyzed and we find that it is well described by a term proportional to  $(\Delta\tau)^4$  consistent with the use of a fourth order path integral factorization of the density matrix<sup>26</sup>.

Assured we are in a low energy regime over the entire range of temperatures considered in this study, we now switch our attention to the structures formed by helium atoms inside the pore. There exists a large literature on the types of phases that are formed when confining a quantum fluid of helium in a cylindrical cavity and a complex phase diagram has been predicted for carbon nanotubes<sup>27–32</sup> and both smooth<sup>33–35</sup> and porous nanopores<sup>36,37</sup>. Advances owing to the development of the WA have allowed this and a previous work<sup>35</sup> to

study considerably larger radius pores at high density and finite temperature in the grand canonical ensemble that approach those studied in recent experiments<sup>14,15</sup>.

For fixed chemical potential  $\mu = -7.2$  K the average volume density  $\rho_V = \langle N \rangle / \pi R^2 L$  inside the nanopore is shown in Figure 3. where  $\langle \dots \rangle$  indicates a thermodynamic average

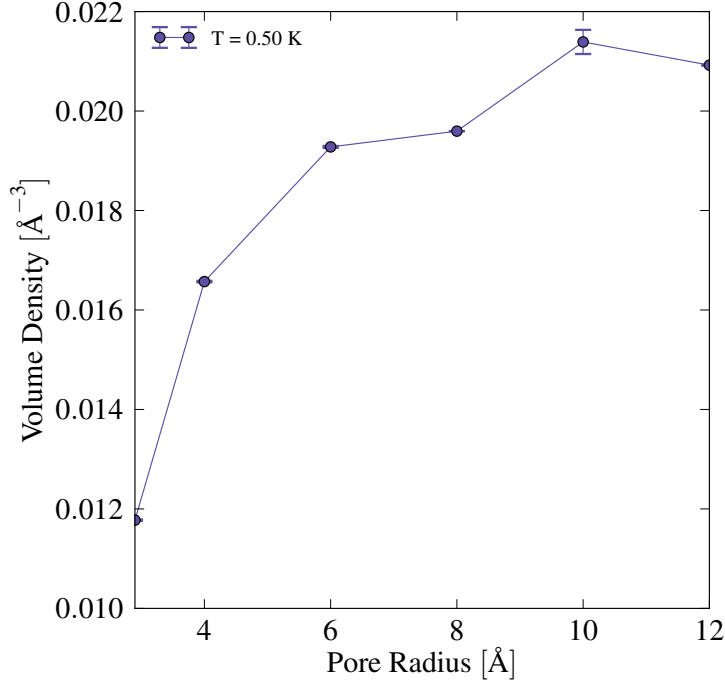


FIG. 3. The average volume density as a function of nanopore radius for helium at saturated vapor pressure and  $T = 0.5$  K.

performed in the quantum Monte Carlo. The observed general trend is an increase in the volume density as a function of radius continuing to a limiting value for large  $R$  that is approaching the expected bulk density of  $0.02198 \text{ Å}^{-3}$ <sup>17</sup>. The resulting phases of helium inside the nanopore can be elucidated by measuring the radial density of particles,  $\rho_R(r)$  defined to be the number of particles found a distance  $r$  from the axis of a pore of radius  $R$  normalized such that the linear density  $\rho_L$  is

$$\rho_L \equiv \frac{\langle N \rangle}{L} = 2\pi \int dr r \rho_R(r) \quad (7)$$

where  $\rho_R(r)$  includes an implicit average over the axial and angular coordinates. The results, shown in Figure 4 display a progression of structures including a nearly one dimensional chain of helium atoms for  $R = 2.9$  Å to a series of three concentric shells surrounding a



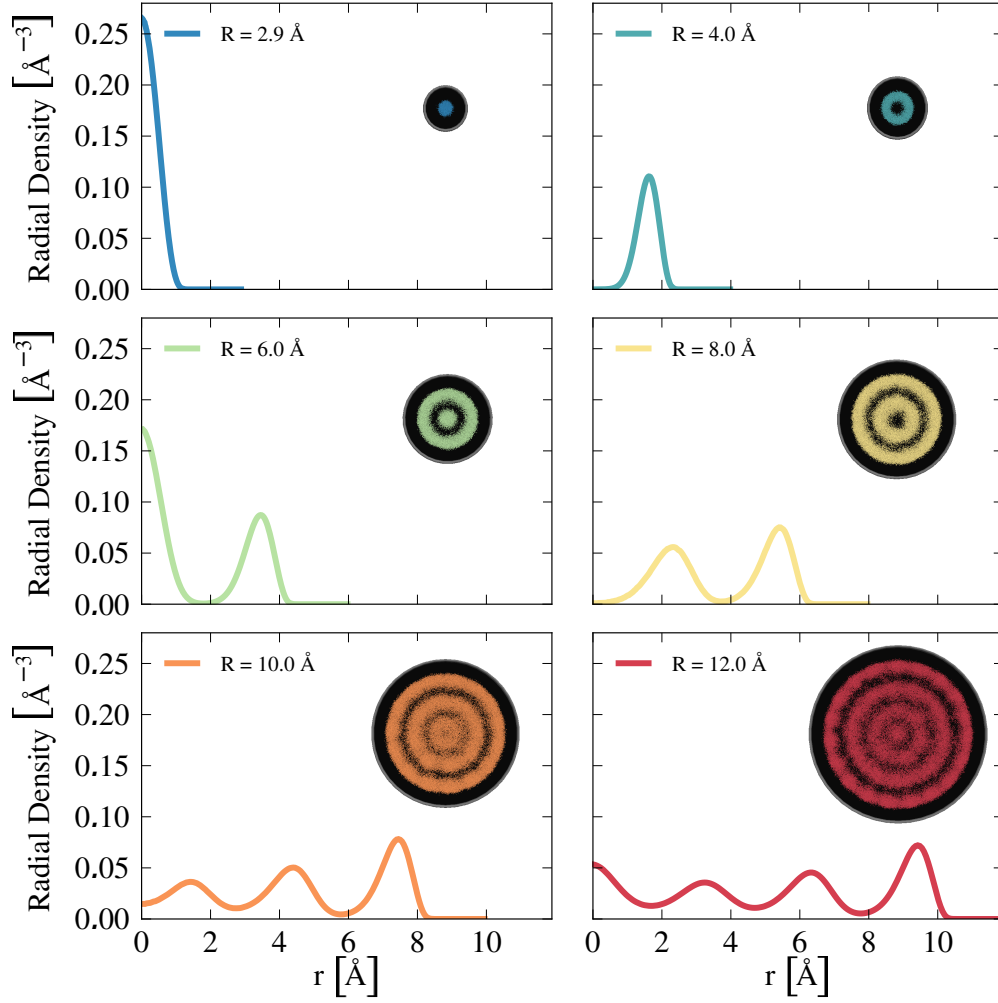


FIG. 4. The radial number density  $\rho_R(r)$  of helium inside nanopores with radii  $R = 2.9, 4.0, 6.0, 8.0, 10.0, 12.0$  Å with an inset showing a full instantaneous worldline configuration inside the pore measured in the quantum Monte Carlo simulations projected on  $z = 0$ . All pores of  $L = 100$  Å and are held at saturated vapor pressure corresponding to  $\mu = -7.2$  K.

chain for  $R = 12.0$  Å. The insets display a snapshot of the discretized helium worldline configuration (space and imaginary time coordinates) from the QMC simulations projected into the  $xy$ -plane at  $z = 0$ .

The observed oscillations in the radial density can be easily understood by contemplating the filling of an empty nanopore through a classical analysis of the potential interactions

only (Figure 1). Beginning with the widest pores, we observe an excluded volume effect due to the *hard*  $\text{Si}_3\text{N}_4$  wall, as well as a deep minimum of the potential near the surface. This will naturally lead to an adsorption effect or wetting of the pore surface with helium atoms forming a shell due to the cylindrical symmetry. As helium atoms continue to enter the pore, the adsorption will cause the area density of the shell to increase until the average separation between atoms inside the shell begins to approach the hard core radius  $r_{\text{hc}}$  of the interaction potential. At this point, it will become energetically favorable to form a new layer inside the one adsorbed on the surface. As this process continues, a series of concentric cylindrical shells may be formed inside the pore analogous to the layering observed in quantum films of bosons<sup>38</sup>.

The results of the radial density for pores of different radii can be separated into two natural groups based on the presence of helium at high linear density near the center of the pore. The existence of such an *inner cylinder* (IC) which can be thought of as a quasi-1D chain of helium atoms for a given radius depends on the details of both the helium-pore and helium-helium interaction potentials. The pore wall (and thus the details of the wall material,  $\text{Si}_3\text{N}_4$  here) produces a region of excluded volume, forcing the helium atoms to remain a distance greater than  $r_e \simeq 1.32 \text{ \AA}$  from the walls of the pore. This sets the location of the outermost shell. The separation between shells is then restricted to be near the minimum of the Aziz potential  $r_m \sim 3 \text{ \AA}$  with some weak dependence on the radius of the pore due to screening of the inner shells. We find that an IC exists whenever the pore radius is approximately divisible by three:  $R = 2.9, 6.0$  and  $12.0 \text{ \AA}$ .

The presence of an IC of helium is intriguing, as we expect that such a quasi-1d bosonic system should lack any long range order down to zero temperature and be described by Luttinger liquid theory. In the next section we test this prediction by introducing the universal theory for an effective harmonic fluid and use it to exhaustively study nanopores with radii  $R = 2.9 \text{ \AA}$  and  $R = 12.0 \text{ \AA}$ .

#### IV. A LUTTINGER LIQUID CORE

In an attempt to understand the relevant low energy degrees of freedom for quasi-1D helium atoms inside the pore, we begin by studying a microscopic Hamiltonian like the one

in Eq. (1) in second quantized form for a strictly one dimensional system of bosons

$$H = \int_0^L dz \left[ \frac{1}{2m} \partial_z \Psi^\dagger(z) \partial_z \Psi(z) + \frac{1}{2} \int_0^L dz' \rho(z) v_{1d}(z - z') \rho(z') \right] \quad (8)$$

where  $\Psi^\dagger(z) = \sqrt{\rho(z)} e^{-i\phi(z)}$  is a bosonic creation operator with  $[\Psi(z), \Psi^\dagger(z')] = \delta(z - z')$  and the 1d density and phase operators satisfy

$$[\rho(z), e^{i\phi(z')}] = \delta(z - z') e^{i\phi(z')}. \quad (9)$$

It is the ability to simulate such microscopic Hamiltonians over a range of energy scales that makes the WA so attractive. The stochastically exact equilibrium properties of a system of strongly interacting bosons at finite temperature can be determined using only fundamental input parameters such as the particle mass  $m$  and the details of the interaction potential.

### A. Luttinger Liquid Theory

The manipulations (generally referred to as bosonization) that transform a microscopic one dimensional interacting Hamiltonian like Eq. (8) into a universal description of the linear hydrodynamics of a quantum fluid (either bosonic or fermionic) are by now standard<sup>6,8,11,39</sup>. In particular, for bosonic systems, Reference 39 provides a detailed and pedagogical derivation of the Luttinger Liquid Hamiltonian defined by

$$H_{LL} - \mu N = \frac{1}{2\pi} \int_0^L dz \left[ v_J (\partial_z \phi)^2 + v_N (\partial_z \theta)^2 \right], \quad (10)$$

where we have included only those terms which are formally relevant in the renormalization group sense. The velocities  $v_J$  and  $v_N$  are fixed by the microscopic details of the underlying high energy model and the angular field  $\theta(z)$  appears through the redefinition of the density operator

$$\rho(z) \equiv \left[ \rho_0 + \frac{1}{\pi} \partial_z \theta(z) \right] \sum_{m=-\infty}^{\infty} e^{i2m\theta(z)} \quad (11)$$

where  $\rho_0$  is the number density at  $T = 0$  in the thermodynamic limit. The underlying bosonic symmetry requires that Eq. (11) in conjunction with Eq. (9) produces the following commutation relation

$$[\partial_z \theta(z), \phi(z')] = i\pi \delta(z - z'). \quad (12)$$

If the system described by Eq. (10) exhibits Galilean invariance we can identify

$$v_J = \frac{\pi\rho_0}{m}, \quad (13)$$

$$v_N = \frac{1}{\pi\rho_0^2\kappa} \quad (14)$$

where  $\kappa$  is the adiabatic compressibility in the limit  $L \rightarrow \infty$ ,  $T \rightarrow 0$ <sup>6</sup>. The connection of these effective velocities to the underlying microscopic details of the original interacting Hamiltonian is now clear: a highly incompressible state with  $v_N \gg 1$  should have a nearly constant density and thus  $\partial_z\theta(z) \sim 0$  whereas a state displaying phase coherence has  $\partial_z\phi(z) \sim 0$  and thus at  $T = 0$  there should be a finite superfluid fraction with  $v_J \gg 1$ .

For a system with periodic boundary conditions in the  $z$ -direction, our original boson field must satisfy  $\Psi^\dagger(z+L) = \Psi^\dagger(z)$  leading to a mode expansion of  $\theta(z)$  and  $\phi(z)$  indexed by wavevector  $q = 2\pi n/L$  where  $n$  is an integer<sup>6</sup>

$$\theta(z) = \theta_0 + \frac{\pi z}{L}(N - N_0) - i \left( \frac{v_J}{v_N} \right)^{1/4} \sum_{q \neq 0} \left| \frac{\pi}{2qL} \right|^{1/2} e^{iqz} (b_q^\dagger + b_{-q}) \text{sgn}(q), \quad (15)$$

$$\phi(z) = \phi_0 + \frac{\pi Jz}{L} - i \left( \frac{v_J}{v_N} \right)^{-1/4} \sum_{q \neq 0} \left| \frac{\pi}{2qL} \right|^{1/2} e^{iqz} (b_q^\dagger - b_{-q}). \quad (16)$$

Here,  $b_q^\dagger$  ( $b_q$ ) is a bosonic creation (annihilation) operator for modes corresponding to long wavelength density fluctuations and the operator  $J$  has even integer eigenvalues indexing the topological winding number of the phase field  $\phi(z)$ ,  $N_0 = \rho_0 L$  and  $N$  is the boson number operator. Substituting Eqs. (15) and (16) into (10) yields the mode expanded Hamiltonian

$$H_{LL} - \mu N = \frac{\pi v}{2KL} J^2 + \frac{\pi v K}{2L} (N - N_0)^2 + \sum_{n \neq 0} v |q| b_q^\dagger b_q, \quad (17)$$

where we have dropped a non-universal constant and defined a new velocity  $v = \sqrt{v_J v_N}$  measuring the famous linear dispersion of the low energy density modes. We have introduced the Luttinger parameter  $K = \sqrt{v_N/v_J}$ <sup>40</sup> and although it is well known that no quantum phase transition can occur as a function of interactions in a truly 1d system described by Eq. (17),  $K$  can be tuned to initiate a  $T = 0$  crossover between a state with algebraic density wave order at  $K = \infty$  to one with quasi-long range superfluid correlations at  $K = 0$ .

The advantages of having the Hamiltonian in this form are unmistakable due to its quadratic nature and the ease with which we can compute averages in the oscillator basis. For example, one can exactly determine the grand partition function  $\mathcal{Z} = \text{Tr} \exp[-(H_{LL} -$

$\mu N)/T]$  in terms of known special functions<sup>41</sup> allowing for the straightforward (although possibly tedious) calculation of all two body correlation functions and thermodynamic observables in terms of the temperature  $T$ , system size  $L$ , Luttinger velocity  $v$  and Luttinger parameter  $K$ . We will focus on the derivation of a single observable, the density-density correlation function  $\langle \rho(z)\rho(0) \rangle$ . Such density correlations are of great interest, as they are easily measured in numerical simulations and are related via a Fourier transform to the experimentally measurable structure factor. In addition, their form provides an intuitive qualitative picture of the types of fluctuations (phase or density) which are dominant. This knowledge can help to pinpoint which region of the 1d crossover phase diagram a given system resides in. Starting from the definition of the density operator in Eq. (11) we have (keeping only the slowest decaying terms)

$$\langle \rho(z)\rho(0) \rangle \approx \rho_0^2 + \frac{1}{\pi^2} \langle \partial_z \theta(z) \partial_z \theta(0) \rangle + 2\rho_0^2 \langle e^{2i\theta(z)} e^{-2i\theta(0)} \rangle. \quad (18)$$

Next, using the mode expansion for  $\theta(z)$  in Eq. (15) the expectation values can be computed to give<sup>35</sup>

$$\begin{aligned} \langle \rho(z)\rho(0) \rangle = \rho_0^2 + \frac{1}{2\pi^2 K} \frac{d^2}{dz^2} \ln \theta_1 \left[ \frac{\pi z}{L}, e^{-\pi v/LT} \right] \\ + \mathcal{A} \cos(2\pi \rho_0 z) \left\{ \frac{2\eta\left(\frac{iv}{LT}\right) e^{-\pi v/6LT}}{\theta_1\left(\frac{\pi z}{L}, e^{-\pi v/LT}\right)} \right\}^{2/K} \end{aligned} \quad (19)$$

where  $\theta_1(x, y)$  and  $\eta(is)$  are the first Elliptical Theta function and Dedekind Eta function respectively.  $\mathcal{A}$  is a non-universal constant dependent on the short-distance properties of the system. Although Eq. (19) may appear daunting at first glance, in the thermodynamic limit  $LT/v \rightarrow \infty$ , it simplifies to<sup>6</sup>

$$\langle \rho(z)\rho(0) \rangle \rightarrow \rho_0^2 - \frac{1}{2\pi^2 K z^2} + \frac{\mathcal{A}}{z^{2/K}} \cos(2\pi \rho_0 z) \quad (20)$$

where it is now clear that  $K \gg 1$  corresponds to a strong tendency towards density wave order.

We are now in a position to test the prediction that for some special radii, the core of a helium-4 filled nanopore can be fully described by Luttinger liquid theory. We can directly compare the pair correlation function measured in the quantum Monte Carlo with the Luttinger liquid prediction of Eq. (19). Before doing so, let us make a brief digression to study the connection between the interactions in the truly one dimensional Hamiltonian in

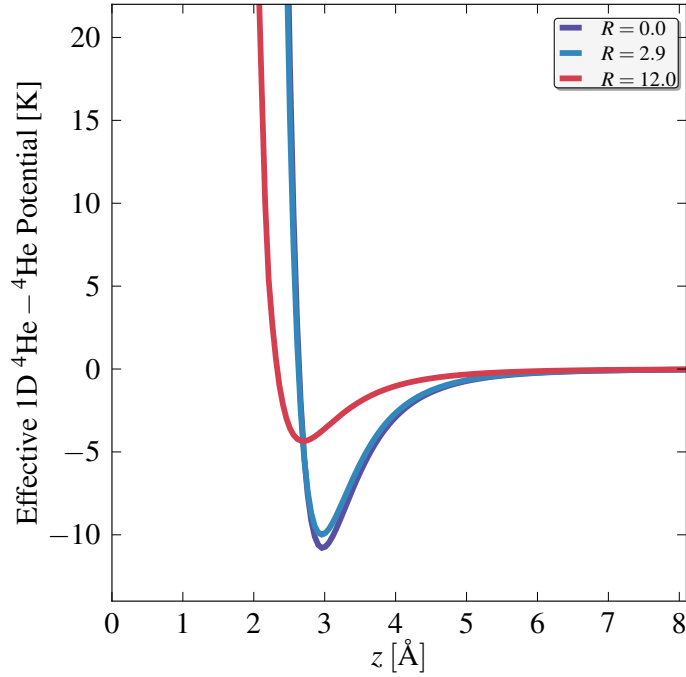


FIG. 5. The effective interaction energy between two helium atoms in strictly one dimension (lowest curve) as well as for the narrowest ( $R = 2.9$  Å) and widest ( $R = 12.0$  Å) pores considered in this study. The radial density used in the numerical evaluation of Eq. (21) was measured at  $T = 0.5$  K, but the form of the potential is only weakly dependent on temperature when  $T < 1.0$  K.

Eq. (8) and those experienced by helium atoms inside the quasi-one-dimensional environment inside the nanopore.

### B. Effective Interactions and Linear Density in the Inner Cylinder

The full interaction and external potentials inside the nanopore defined in Eqs. (2) and (4) and displayed in Figure 7 can be related to the 1d potential of Eq. (8) through

$$v_{1d}(z) = \frac{1}{\rho_L^2} \int d^2r \int d^2r' v(\mathbf{r} - \mathbf{r}') \rho_R(r) \rho_R(r') \quad (21)$$

where  $\mathbf{r} = (r, \varphi, z)$  is a vector in cylindrical coordinates and  $\rho_R(r)$  is the radial density defined in Eq. (7). The form of this effective interaction potential can be investigated using the measured data from our QMC simulations with the results shown in Figure 5. We observe that the effective potential in the  $R = 2.9$  Å pore very closely reproduces the

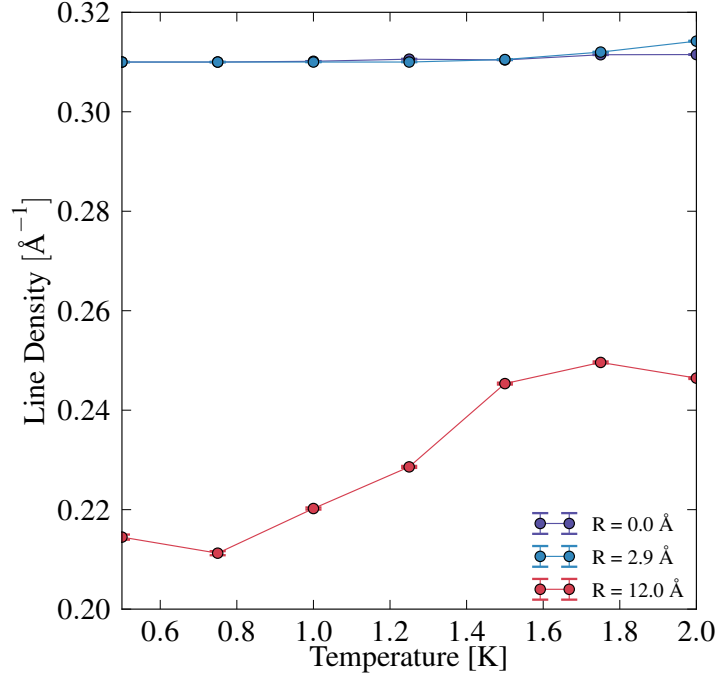


FIG. 6. The number of particles per angstrom for helium atoms in strictly one dimension (with  $\mu = 85$  K), a pore with  $R = 2.9$  Å and inside the inner cylinder with  $r < r_{IC} = 1.75$  Å for  $R = 12.0$  Å. All pores have length  $L = 100$  Å and the finite radius pores are held at saturated vapor pressure with  $\mu = -7.2$  K.

interactions that would be experienced in a system of helium atoms interacting in strictly one dimension ( $R = 0$ ). For the largest radius pore of  $R = 12.0$  Å however, screening from the concentric shells leads to a potential with a much weaker minimum (about half the depth of the unscreened bulk Aziz potential) with its location shifted to smaller separations. The effective 1d interactions in the axial direction experienced by atoms in the center of the pore influences the average separation between atoms which can be determined from the average linear density in Figure 6. We observe almost no temperature dependence for small radii and the agreement of the linear density for  $R = 0$  and  $R = 2.9$  Å is by design, with the chemical potential having been tuned to  $\mu_{\text{SVP}} - V(0; 2.9) \simeq 85$  K for the one dimensional ( $R = 0$ ) system to reproduce the energetic confinement displayed in Figure 1 at low temperature. The numerical value of  $\rho_0$ , defined as the zero temperature thermodynamic limit of the linear density in the core is measured to be  $\rho_{0,0} \simeq \rho_{0,2.9} = 0.3100(1)\text{Å}^{-1}$  (with the number in brackets indicating the uncertainty in the final digit and a second subscript being the pore

radius in angstroms). The fact that this value is slightly smaller than  $r_{\min}^{-1}$  can be attributed to quantum effects. For  $R = 12.0 \text{ \AA}$ , the observed density of  $\rho_{0,12} = 0.2144(5) \text{ \AA}^{-1}$  is only weakly related to the minimum of the effective 1d potential shown in Figure 5 as there is a temperature dependent amount of exchange of helium atoms between the inner cylinder and surrounding shells.

### C. Density Correlations

Having studied the effective one dimensional potential felt by helium atoms inside the pore, and determined the linear density in the inner cylinder we are now in a position to evaluate the efficacy of Eq. (19) in describing density correlations in the nanopore. A first glance at this expression indicates that there are *four* fitting parameters,  $(\rho_0, v, K, \mathcal{A})$  to be determined; a number that would seemingly allow large flexibility (and thus limited accuracy) of any least squares fitting procedure. However, one of the most attractive features of Eq. (19) is that it provides a prediction for the full analytical form of the finite size and temperature scaling behavior of  $\langle \rho(z)\rho(0) \rangle$ , a rare luxury indeed. We thus have a stringent procedure for confirming Luttinger liquid behavior in the nanopore: (1) perform simulations for different pore radii, lengths and temperatures measuring thermodynamic estimators and correlation functions. (2) The average linear density in the central region of the pore can be determined as a function of temperature and extrapolated for each  $L$  and  $R$  to  $T = 0$ , this fixes  $\rho_{0,R}$ . (3) For each radius which displays a finite density of helium atoms at  $r = 0$ , perform a least squares fit of the density-density correlation function measured in the QMC to Eq. (19) at a single  $L$  and  $T = 0.5 \text{ K}$  (the lowest temperature measured). This fixes the remaining three parameters,  $v_R$ ,  $K_R$  and  $\mathcal{A}_R$  where the subscript  $R$  will be used to distinguish results for different finite radius pores. These parameters are *intrinsic* to the zero temperature thermodynamic limit of Eq. (10) and provided that helium-4 inside the core is behaving as a LL, *cannot* exhibit any temperature dependence. (4) In other words, for a given radius, a single fit to Eq. (19) at fixed temperature and system size is enough to compute the LL prediction for the pair correlation function at all other temperatures and sizes and we explore the resulting predictions for  $R = 0, 2.9$  and  $12.0 \text{ \AA}$  below. Obviously we are constrained by the low energy, long wavelength region of applicability of  $H_{\text{LL}}$  assumed throughout this study and it is easily confirmed that deviations appear at short lengths and



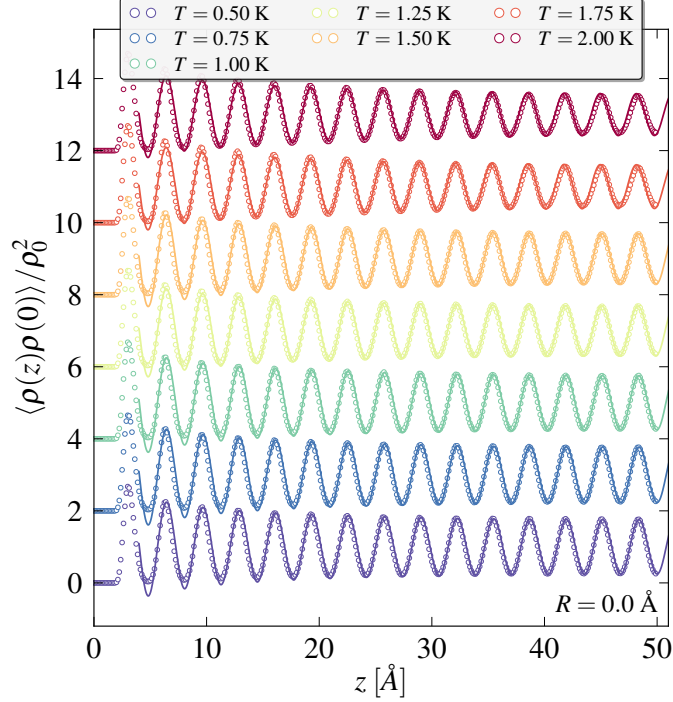


FIG. 7. Simulation data (circles) and a fit to Eq. (19) (lines) for the pair correlation function of strictly one dimensional helium atoms ( $R = 0$ ). The chemical potential ( $\mu = 85$  K) has been set to approximate the energetically confining environment coming from the pore wall (see text). Error bars are smaller than the symbol size and data in the main panel has been given a vertical  $T$ -dependent shift for clarity with  $T = 0.5$  K at the bottom and  $T = 2.0$  K at the top.

high temperature.

To orient ourselves we begin by studying the strictly one dimensional system, which we fully expect to be well described by LL theory. In Figure 7 we plot the results of QMC simulations for the density-density or pair correlation function (symbols) for a chain of helium atoms with  $L = 100$  Å and  $\mu = 85$  K.

Performing the aforementioned fits at  $T = 0.5$  K, we find  $v_0 = 75(1)$  ÅK and  $K_0 = 6.4(3)$  where stochastic errors in QMC data produce uncertainty in our regression procedure. The exact value of  $\mathcal{A}_l$  is not relevant in the subsequent discussion and it will not be mentioned further. Fixing all parameters, Eq. (19) was used to produce the solid lines in Figure (7) where a vertical shift has been included to allow for the visual differentiation of the effects of temperature. We observe spectacular agreement over the entire range of temperatures considered, noting that no additional fitting was required above  $T = 0.5$  K. We now perform

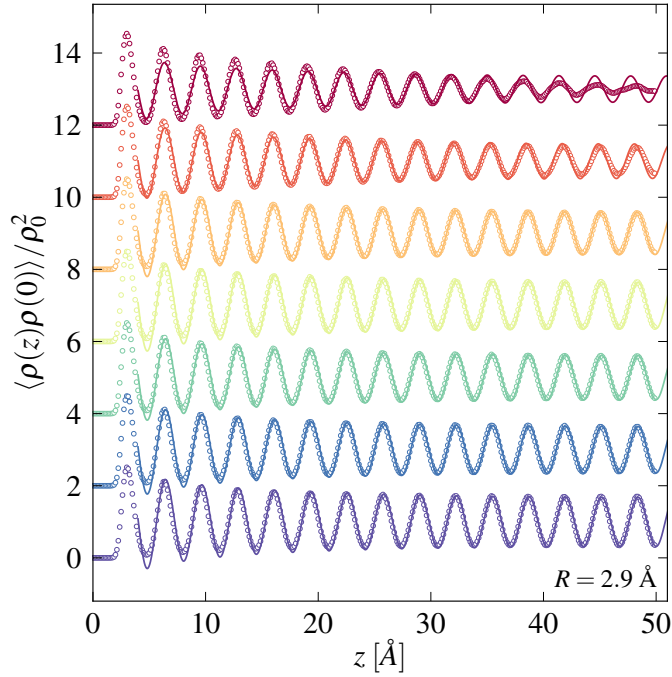


FIG. 8. Simulation data (symbols) and a fit to Eq. (19) (lines) for the pair correlation function along the axis of a nanopore with  $R = 2.9 \text{ \AA}$  and  $L = 100 \text{ \AA}$ . Different curves correspond to increasing temperature from  $T = 0.5 \text{ K}$  (bottom) to  $T = 2.0 \text{ K}$  (top) (vertical shifts have been added for clarity) with the legend displayed in Figure 7.

an identical procedure for the narrowest finite radius pore,  $R = 2.9 \text{ \AA}$ , with the results for the density-density correlation function shown in Figure 8. Similar to the case of 1d helium ( $R = 0$ ), we observe persistent oscillations out to the largest distances possible in the  $L = 100 \text{ \AA}$  pore with periodic boundary conditions indicating a strong tendency towards density wave order. As the helium-pore interaction is independent of the axial coordinate  $z$  and the radial density for  $R = 2.9 \text{ \AA}$  (Figure 4) exhibits only a single central chain of atoms, Galilean invariance further restricts the ratio  $v_{2.9}/K_{2.9} = \pi\rho_{0,2.9}/m^6$ . Extracting values in the presence of this constraint at  $T = 0.5 \text{ K}$  yields  $v_{2.9} = 70(3) \text{ \AA K}$  and  $K_{2.9} = 6.0(2)$ , in close agreement with the 1d chain of helium atoms as expected. For the finite radius pore however, we begin to observe deviations from LL predictions both at small distances and high temperature. Once the relevant thermal lengthscale,  $\ell_T \sim v/T$  is on the order of the pore diameter, the system can no longer be thought of as quasi-1d and we expect significant corrections to arise from the thermal excitation of transverse modes. The values

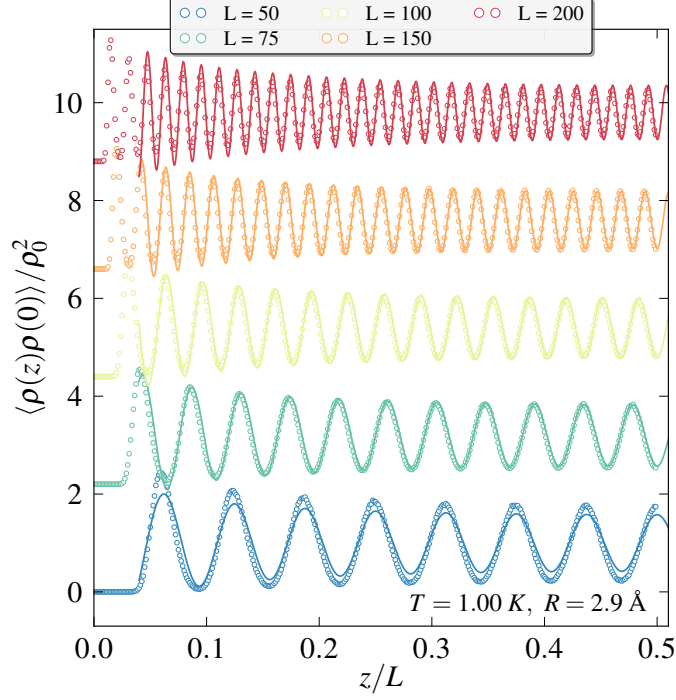


FIG. 9. Simulation data (symbols) and a fit to Eq. (19) (lines) for the pair correlation function along the axis of a nanopore with  $R = 2.9 \text{ \AA}$  for various pore lengths  $L$  (increasing from bottom to top). As in previous figures, a vertical shift has been added to distinguish the curves and accentuate the scaling behavior. Note the use of a dimensionless abscissa in order to plot spatial correlations for different pore lengths on the same scale.

of the LL velocity and interaction strength determined in this way can also be used to test the predicted finite size scaling of Eq. (19) at fixed  $T = 1.0 \text{ K}$  as seen in Figure 9. We stress that the nearly perfect agreement seen between simulation data and LL theory in Figure 9 for  $L \geq 75$  does not require any additional fitting parameters and is a direct consequence of the predictive power of the universal hydrodynamics of  $H_{\text{LL}}$ .

Shifting attention to the  $R = 12.0 \text{ \AA}$  pore, in order to make an effective comparison we will focus the analysis on only those helium atoms which spontaneously find themselves inside the inner cylinder. The precise definition of which helium atoms are inside the IC is somewhat arbitrary, but we define this to coincide with the location of the first minimum in the radial density in the presence of finite density at  $r = 0$ . For the pores considered here, this corresponds to  $r_{\text{IC}} = 1.75 \text{ \AA}$ . We expect that the presence of particle exchanges between the central chain of helium atoms and the surrounding cylindrical shells should

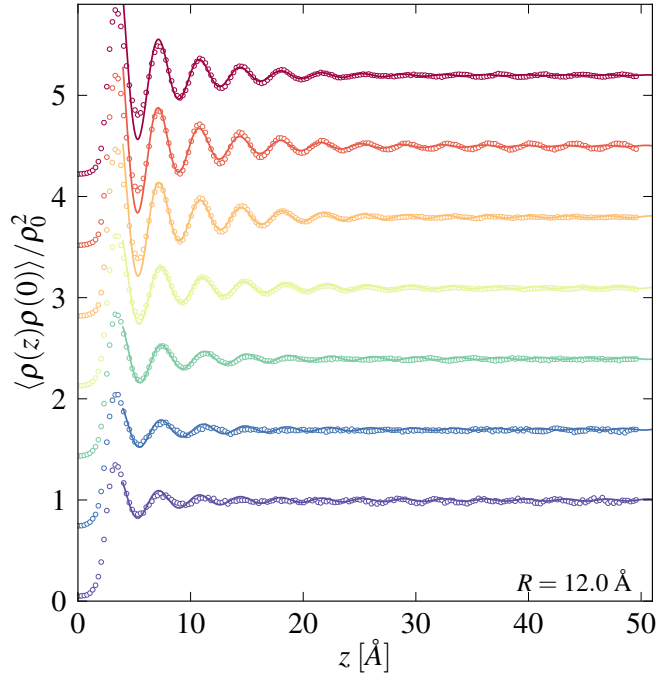


FIG. 10. Simulation data (symbols) and a fit to Eq. (19) (lines) for the inner cylinder pair correlation function along the axis of a nanopore with  $L = 100 \text{ \AA}$  and  $R = 12.0 \text{ \AA}$  for helium atoms with  $r < r_{\text{IC}} = 1.75 \text{ \AA}$ . The curves have been shifted for clarity and correspond to increasing temperature from  $T = 0.5 \text{ K}$  (bottom) to top  $T = 2.0 \text{ K}$  (top) with the legend displayed in Figure 7.

begin to play an important role in the ‘melting’ of the quasi-long range density wave order observed in narrow pores. The resulting axial pair correlation function measured in our QMC simulations is shown in Figure 10. The data show density-density correlations in the inner cylinder that decay much faster than those seen for  $R = 2.9 \text{ \AA}$ . The lack of Galilean invariance due to atoms in the surrounding concentric shells adds some additional freedom to the now familiar fitting procedure (and thus more uncertainty) and it has been determined that  $v_{12} = 42(2) \text{ \AA K}$  and  $K_{12} = 1.3(2)$ . This value of the Luttinger parameters is nearly a factor of five smaller than that found for the strictly one dimensional system and indicates that this nanopore is in a region of phase space starting to be dominated by superfluid fluctuations.

The success of the Luttinger liquid prediction for  $\langle \rho(z)\rho(0) \rangle$  in Eq. (19) in describing the density-density correlations measured in our quantum Monte Carlo simulations is convincing

TABLE I. Values for the Luttinger velocity and parameter for helium atoms in 1d and in the quasi-1d core of nanopores by comparing the Luttinger liquid prediction with quantum Monte Carlo measurements of the pair correlation function. The number in brackets indicates the uncertainty in the final digit.

Radius $R$ [Å]	Luttinger Velocity $v$ [ÅK]	Luttinger Parameter $K$
0.0	75(1)	6.4(3)
2.9	70(3)	6.0(2)
12.0	42(2)	1.3(1)

evidence that a quantum fluid of helium-4 in pores with  $R < 3$  Å can be described by LL theory and that the central region of wider pores may display emergent harmonic fluid-like properties. In the next section, we discuss the implications of these results and argue that the determination of  $K$  and  $v$  for a given system is not simply an academic exercise but has real consequences for the stability of the Luttinger liquid phase.

## V. DISCUSSION

Although it appears that LL theory works exceedingly well in describing pair or density-density correlations for the finite radius pores considered in this study, it is natural to ask whether there is something special about this particular observable. As mentioned in Section IV A the utility of the harmonic fluid description of 1d systems is that the resulting mode expanded Hamiltonian of Eq. (17) is quadratic (neglecting formally irrelevant operators) and thus the full grand partition function can be computed in closed form. We can therefore compare other two body correlation functions computed within Luttinger liquid theory with those measured in the QMC using the values of  $v_R$  and  $K_R$  determined in this study and displayed in Table I. We have measured the axial one body matrix  $n(z) = \langle \Psi^\dagger(z) \Psi(0) \rangle$  in the QMC<sup>17</sup> and find acceptable agreement with LL theory (with no new fitting parameters) at low  $T$ . The large value of  $K \approx 6$  for  $R = 0$  and  $R = 2.9$  Å adds some complications when comparing numerical results for some scalar (non-correlation function) observables with predictions coming from bosonization. For example, the strong tendency towards density wave order  $\partial_z \theta(z) \sim 0$  displayed in Figures 7-8 points to a compressibility  $a\kappa \sim \langle N^2 \rangle - \langle N \rangle^2 \approx 0$

and thus an analysis of the probability distribution function for particle number fluctuations like the one performed in Reference 41 is not feasible. The conjugate relationship between density and phase variables in the LL theory (Eq. (12)) would predict that the boson phase  $\phi(z)$  should be totally disordered resulting in a vanishing superfluid density which is observed in the numerics.

For the  $R = 12$  Å pore, the analysis presented in the previous section is based on a fraction of the total number of  $^4\text{He}$  atoms in the pore, those that dynamically have  $r < r_{\text{IC}}$  and find themselves in the core of the nanopore. The justification for this originates in the idea that we may be able to regard the pore as a coupled multi-component LL, with cylindrical shells replacing the legs of previously studied ladders<sup>42</sup>. Guided by these results we assume that only a single gapless degree of freedom may survive as a “center of mass mode” in the low energy effective field theory, due to tunneling between the shells. In the nanopore, this tunneling has two origins corresponding to the physical mobility of particles between shells as well as multi-particle quantum exchange cycles which may dynamically connect them at short time scales.

With this in mind, let us re-analyze the slight discrepancies between the quantum Monte Carlo data in Figure 10 and LL theory. At the lowest temperature considered,  $T = 0.5$  K, the simulation data appears to show oscillations with a period that is slightly larger than that predicted by  $1/(2\pi\rho_{0,12})$ . This is most likely attributed to the physical exchange of particles between the inner cylinder and the surrounding shells producing a greater uncertainty in  $\rho_{0,12}$  than is reflected in errorbars and making the extrapolation to zero temperature a difficult task. The amplitude of the oscillations in the pair correlation function is also slightly overestimated by LL theory at low temperature. Again, the finite radius of the pore is to blame, resulting in a finite superfluid fraction of helium (as measured via the usual winding number estimator<sup>19</sup> along the axis of the pore) of  $\rho_s/\rho_0 \sim 0.2$  at  $T = 1.0$  K. Transverse degrees of freedom that are not frozen out at this temperature lead to an increase in multi-particle exchanges that enhance superfluidity in the nanopore.

The opposite behavior appears to occur at high temperature with the simulation data showing weaker decay than predicted by LL theory with thermal fluctuations being unable to fully quench the proclivity towards density wave order. This is the opposite effect observed for  $R = 2.9$  Å in Figure 8 and it can possibly be explained through stabilization of the IC from attraction with surrounding atoms.

In a previous work<sup>41</sup>, finite size corrections to  $\rho_{0,R}$  arising from the inclusion of higher order formally irrelevant terms in the effective Hamiltonian of Eq. (10) have been discussed at great length. However, due to the relatively large energy scales at play in the nanopore (Figure 2) they are less important here and are not major players in any observed discrepancies between simulation data and the effective field theory.

We observe a general trend of  $K$  decreasing with increasing pore radius as seen in Table I. However, the actual numerical values of the Luttinger parameter  $K$  for pores of varying radius can provide important information on the sensitivity of the LL to perturbations coming from commensuration effects or disorder; both of which are surely present in the real experiments of Savard *et al.*<sup>14,15</sup>. For a strictly one dimensional system, the introduction of a weak periodic substrate that is commensurate with the density will only lead to complete localization and the destruction of the harmonic fluid if  $K > 1/2$ <sup>6</sup>. Commensuration at other wavevectors is less relevant and would require a greater value of  $K$  to destabilize the LL. The introduction of a weak disorder potential, as might be present near the glassy walls of the pore, is known to be relevant only when  $K > 2/3$ <sup>43</sup>.

For the narrowest pores considered in this study  $R < 3$  Å, we have found a value of  $K \approx 6$  at saturated vapor pressure, indicating a strong tendency to form a solid, resulting from strong confinement and the deep minimum and accompanying hardcore found in the effective interaction potential  $v_{1d}(z)$ . The experimental confirmation of this result could be accomplished by noting that the formation of a quasi-solid should impede superfluid flow through a helium-4 filled nanopore at low temperature.

It may be useful to compare the values of  $K_R$  found here with other studies of low dimensional helium. For example, in a WA study of helium-4 confined to flow in the channels formed by screw dislocations with  $R \sim 3$  Å in solid helium, it was found that  $K = 0.205(20)$ <sup>44</sup>, nearly thirty times smaller than the comparable value of  $K_{2.9}$  measured in this study. The sources of the discrepancy are rooted in the “softness” of the confining potential inside the screw dislocation as helium atoms are able to penetrate into the surrounding solid held at  $\mu = 0.02$  K corresponding to the bulk melting point.

Much exciting work remains to be done in the nanopore system including a more systematic study of the superfluid density which can be measured in bundles of tubes or pores via torsional oscillator techniques<sup>45,46</sup>. The construction of more realistic models that contain both commensuration and disorder potentials would also enhance the applicability of

numerical simulations. Further exploration of the available parameter space is also in order, including altering the chemical potential at fixed radius to simulate the effects of pressure which can be freely tuned in experiments.

In conclusion, we have studied a quantum fluid of bosonic helium-4 confined inside nanopores of varying radii via large scale continuum Worm Algorithm quantum Monte Carlo Simulations at saturated vapor pressure below the bulk superfluid transition temperature. The results show a progression of phases inside the pore exhibiting a possible quasi-one-dimensional core surrounded by concentric shells of helium depending on the radius. When the core of the nanopore has a non-zero density of helium, the finite temperature and scaling properties of the density-density correlation function are fully described within harmonic Luttinger liquid theory. The description of the emergent low energy phase of confined helium in terms of the harmonic field theory allows for the extraction of the Luttinger parameter  $K$  which is found to be a decreasing function of radius. As the pore radius increases, the inner helium core is screened from the confining effects of the pore wall by the surrounding matter, resulting in a pronounced enhancement of quantum exchanges leading to superfluidity. The precise relationship between the material through which the pore has been sculpted and the resulting Luttinger liquid parameters could be further explored leading to new predictions and optimized experiments with the maximum likelihood of detecting a universal and stable one-dimensional quantum harmonic fluid of helium at low temperature.

## ACKNOWLEDGMENTS

The author would like to thank I. Affleck, M. Boninsegni and G. Gervais for many ongoing discussions. This work was made possible through computational resources provided by the National Resource Allocation Committee of Compute Canada with all simulations taking place on Westgrid or SHARCNET.

---

<sup>1</sup> E. H. Lieb and W. Liniger, Phys. Rev. **130**, 1605 (1963).

<sup>2</sup> S.-I. Tomonaga, Prog. Theor. Phys. **5**, 544 (1951).

<sup>3</sup> D. C. Mattis and E. H. Lieb, J. Math. Phys. **6**, 304 (1965).

<sup>4</sup> A. Luther and I. Peschel, Phys. Rev. B **9**, 2911 (1974).



- <sup>5</sup> K. B. Efetov and A. I. Larkin Zh. Eksp. Teor. Fiz. **69** 764 (1975).
- <sup>6</sup> F. D. M. Haldane, Phys. Rev. Lett. **47**, 1840 (1981).
- <sup>7</sup> F. D. M. Haldane, J. Phys. C: Sol. State Phys. **14**, 2585 (1981).
- <sup>8</sup> T. Giamarchi, *Quantum Physics in One Dimension* (Oxford University Press, Oxford, 2004).
- <sup>9</sup> M. Greiner, I. Bloch, O. Mandel, T. Hansch, and T. Esslinger, Phys. Rev. Lett. **87**, 160405 (2001).
- <sup>10</sup> C. Ryu, M. Andersen, P. Cladé, V. Natarajan, K. Helmerson, and W. Phillips, Phys. Rev. Lett. **99**, 260401 (2007).
- <sup>11</sup> M. Cazalilla, R. Citro, T. Giamarchi, E. Orignac, and M. Rigol, Rev. Mod. Phys. **83**, 1405 (2011).
- <sup>12</sup> J. R. Beamish, A. Hikata, L. Tell and C. Elbaum, Phys. Rev. Lett. **50**, 425 (1983).
- <sup>13</sup> J. Taniguchi, Y. Aoki and M. Suzuki, Phys. Rev. B **82**, 104509 (2010).
- <sup>14</sup> M. Savard, C. Tremblay-Darveau, and G. Gervais, Phys. Rev. Lett. **103**, 104502 (2009).
- <sup>15</sup> M. Savard, G. Dauphinais, and G. Gervais, Phys. Rev. Lett. **107**, 254501 (2011).
- <sup>16</sup> M. Boninsegni, N. V. Prokof'ev, and B. V. Svistunov, Phys. Rev. Lett. **96**, 070602 (2006).
- <sup>17</sup> M. Boninsegni, N. V. Prokof'ev, and B. V. Svistunov, Phys. Rev. E **74**, 036701 (2006).
- <sup>18</sup> D. Ceperley, Rev. Mod. Phys. **67**, 279 (1995).
- <sup>19</sup> E. Pollock and D. Ceperley, Phys. Rev. B **36**, 8343 (1987).
- <sup>20</sup> R. A. Aziz, V. Nain, J. S. Carley, W. L. Taylor, and G. T. McConville, J. Chem. Phys. **70**, 4330 (1979).
- <sup>21</sup> G. Tjatjopoulos, D. Feke, and J. Mann Jr, J. Phys. Chem. **92**, 4006 (1988).
- <sup>22</sup> J. A. Wendel and W. A. Goddard, J. Chem. Phys. **97**, 5048 (1992).
- <sup>23</sup> C. Chakravarty, J. Phys. Chem. B **101**, 1878 (1997).
- <sup>24</sup> W.-Y. Ching, Y.-N. Xu, J. D. Gale, and M. Rühle, J. Am. Ceram. Soc. **81**, 3189 (1998).
- <sup>25</sup> M. Boninsegni, J. Low Temp. Phys. **160**, 441 (2010).
- <sup>26</sup> S. Jang, S. Jang, and G. A. Voth, J. Chem. Phys. **115**, 7832 (2001).
- <sup>27</sup> G. Stan and M. W. Cole, Surface Science **395**, 280 (1998).
- <sup>28</sup> S. M. Gatica, G. Stan, M. M. Calbi, J. K. Johnson and M. W. Cole, J. Low T. Phys. **120**, 337 (2000).
- <sup>29</sup> M. W. Cole, V. H. Crespi, G. Stan, C. Ebner, J. M. Hartman, S. Moroni, and M. Boninsegni, Phys. Rev. Lett. **84**, 3883 (2000).

- <sup>30</sup> M. Gordillo, J. Boronat, and J. Casulleras, Phys. Rev. B **61**, R878 (2000).
- <sup>31</sup> M. Gordillo, J. Boronat, and J. Casulleras, Phys. Rev. B **76**, 193402 (2007).
- <sup>32</sup> M. C. Gordillo and J. Boronat, J. Low Temp. Phys. **157**, 296 (2009).
- <sup>33</sup> N. M. Urban and M. W. Cole, Int. J. Mod. Phys. B **20**, 5264 (2006).
- <sup>34</sup> E. S. Hernández, J. Low Temp. Phys. **162**, 583 (2010).
- <sup>35</sup> A. Del Maestro, M. Boninsegni, and I. Affleck, Phys. Rev. Lett. **106**, 105303 (2011).
- <sup>36</sup> M. Rossi, D. Galli, and L. Reatto, Phys. Rev B **72**, 064516 (2005).
- <sup>37</sup> M. Rossi, D. E. Galli, and L. Reatto, J. Low Temp. Phys. **146**, 95 (2006).
- <sup>38</sup> B. Clements, J. Epstein, E. Krotscheck, and M. Saarela, Phys. Rev. B **48**, 7450 (1993).
- <sup>39</sup> M. A. Cazalilla, J. Phys. B: At. Mol. Opt. Phys. **37**, S1 (2004).
- <sup>40</sup> Two predominant definitions of the Luttinger parameter  $K$  exist in the literature corresponding to  $K$  or  $\tilde{K} = 1/K$ . We have chosen the present definition to be consistent with Reference 35 but we caution the reader to be wary of this ambiguity.
- <sup>41</sup> A. Del Maestro and I. Affleck, Phys. Rev. B **82**, 060515(R) (2010).
- <sup>42</sup> E. Orignac and T. Giamarchi, Phys. Rev. B **57**, 11713 (1998).
- <sup>43</sup> T. Giamarchi and H. J. Schulz, Phys. Rev. B **37**, 325 (1988).
- <sup>44</sup> M. Boninsegni, A. B. Kuklov, L. Pollet, N. V. Prokof'ev, B. V. Svistunov and M. Troyer, Phys. Rev. Lett **99**, 035301 (2007).
- <sup>45</sup> N. Wada, T. Matsushita, M. Hieda, and R. Toda, J. Low Temp. Phys. **157**, 324 (2009).
- <sup>46</sup> N. Wada, Y. Minato, T. Matsushita, and M. Hieda, J. Low Temp. Phys. **162**, 549 (2011).